Overtones of the Si−H Stretching−Bending Polyad in $SiHD_3$: Internal Coordinate Force Field, ab initio Dipole Moment Surfaces, and Band Intensities

Hai Lin* and Hans Bürger

Anorganische Chemie, Fachbereich 9, Universität- Gesamthochschule Wuppertal, D−42097 Wuppertal, Germany

Sheng-Gui He and Lan-Feng Yuan

Open Laboratory of Bond Selective Chemistry, and the Institute for Advanced Studies, University of Science and Technology of China, Hefei, 230026, P. R. China

Jürgen Breidung and Walter Thiel

Max-Planck-Institut für Kohlenforschung, Kaiser-Wilhelm-Platz 1, D−45470 Mülheim an der Ruhr, Germany

Received: January 31, 2001; In Final Form: April 19, 2001

Overtones of the Si−H stretching−bending polyad of the $SiHD_3$ molecule are studied using an internal coordinate force field model. The potential parameters are optimized by fitting to the experimental band centers. The Fermi resonance between the Si−H stretching and bending motions is insignificant due to cancellation of the contributions from kinetic and potential terms. This suggests a slow redistribution of vibrational energy between these two degrees of freedom and induces local mode character of respective vibrations. Band intensities are calculated by using ab initio one- and three-dimensional dipole moment surfaces (DMS). These agree reasonably well with the observations. The successful reproduction of relative intensities between the $(n_1 - 1)\upsilon_1 + 2\upsilon_5$ stretching−bending combination bands and the $n_1\upsilon_1$ stretching bands establishes the importance of the bending motion in the multidimensional DMS for intensity investigations.

Introduction

The dynamics of molecular vibrations have been of interest for some time due to their importance for the development of bond-selective photochemistry. For X−H stretching vibrations, there are two limiting cases: On one hand, local mode behavior is found in some XH_n (X = S, Se, Te; As, Sb, Si; Ge and Sn; n = 2, 3, and 4) molecules[1,2] and their isotopomers, which implies that the vibrational energy remains localized in an individual X−H bond for a long time. On the other hand, the strong Fermi resonance between the C−H stretching and bending motions in CHY_3-type species (Y = D, F, Cl, Br, I, and CF_3)[3−5] leads to a fast intramolecular vibrational redistribution (IVR) between these degrees of freedom. It should be instructive to study the connection between these two extremes.

The $SiHD_3$ molecule provides us some possibilities for this purpose because it is a near-local-mode molecule with an isolated Si−H chromophore that is analogous to the C−H chromophore in CHY_3 species. One might argue that the strong Fermi resonance between the stretching and bending motions is specific for the C−H chromophore because for the other X−H chromophores the stretching fundamentals are far away from the first bending overtones. However, the corresponding energy differences in the $CHBr_3$[4] and CHI_3[5] molecules are also large, while the Fermi resonance is still prominent. Moreover, from the point of view of the internal coordinate force field model,[6−11] there are both kinetic and potential contributions to the Fermi interactions, the former being always present. Therefore, it is desirable to gain deeper insight into this problem.

Another motivation for the present study comes from the modeling of the intensities of the Si−H stretching-bending polyads in $SiHD_3$ as excitation increases. Experiments show that the intensities of the stretching bands decrease rapidly and uniformly from υ_1 to $3\upsilon_1$. However, this trend is interrupted for $4\upsilon_1$, whose intensity is slightly larger than that of $3\upsilon_1$.[12] Moreover, it is usually assumed that only the C−H or X−H stretching motions carry absorption intensity and that the stretching-bending combination bands will borrow some intensity from the pure stretching overtones through resonances. Such an assumption has been successfully applied to CHY_3 species,[3−5] showing that the relative intensities within each Fermi resonance polyad depend largely on the mixing of wave functions through Fermi resonances. It will be interesting to see if this is also true for $SiHD_3$.

As one of the near-local-mode molecules, $SiHD_3$ has been the subject of several low and high-resolution infrared[13−23] and microwave spectroscopic studies.[24,25] The υ_1 state was found to be perturbed by unknown dark states. A definite perturbation was also observed in the $2\upsilon_1$ band when $J' \geq 13$.[13] By contrast, the $6\upsilon_1$, $7\upsilon_1$, $8\upsilon_1$, and $9\upsilon_1$ states were found to be free of perturbations.[17,19,20] The $3\upsilon_1$ and $4\upsilon_1$ states have not yet been described experimentally, but their band origins were predicted theoretically by Wang and Sibert[26] by high-order canonical Van Vleck perturbation theory (CVPT) based on a high-level quartic ab initio force field.[27] According to these authors, the Si−H stretching states in silane and its isotopomers are generally little

* Corresponding author. On leave from Open Laboratory of Bond Selective Chemistry, University of Science and Technology of China, Hefei, 230026, P. R. China. Email: hailin@mpi-muelheim.mpg.de.

10.1021/jp010404t CCC: $20.00
Published on Web 06/02/2001

affected by Si−H bending, although some of them are perturbed by states due to other vibrational combinations.

In this work, we will focus on the Si−H stretching and stretching−bending overtones of $SiHD_3$. Vibrational wavenumbers and intensities of stretching−bending overtones up to 9000 cm^{-1} (including $3\upsilon_1$ and $4\upsilon_1$) will be reported as obtained from Fourier transform infrared (FTIR) spectra recorded in Wuppertal.[12] Transition frequencies and intensities will be studied using a chromophore force field model in terms of internal coordinates. The potential parameters will be optimized by fitting to the experimental band centers. One- and three-dimensional dipole moment surfaces (DMS) will be calculated ab initio. Band intensities will be determined by use of the ab initio DMS and compared with the observations.

Experiment

The spectra of $SiHD_3$ were recorded using a Bruker IFS120HR Fourier transform spectrometer. Details of the overtone spectra will be reported elsewhere.[12] Here we describe only those aspects which are relevant to the present work. The spectra were assigned vibrationally mainly on the basis of the CVPT calculation by Wang and Sibert.[26] The band centers were determined from low-resolution (0.2 cm^{-1}) spectra. For the $3\upsilon_1$ and $4\upsilon_1$ bands, the *J* structure was resolved, and the *K* structure was partly resolved. The band centers were determined by taking advantage of a fit of the $K = 0$ transitions only. The spectra above 3000 cm^{-1} are dominated by overtones of the Si−H stretching υ_1 mode and combinations comprising of the Si−H stretching and other vibrational modes. Among these bands, the Si−H stretching-bending $n_1\upsilon_1 + n_5\upsilon_5$ bands are prominent. Here, n_1 and n_5 are the vibrational quantum numbers of the υ_1 and υ_5 modes, respectively.

The absolute intensities of the FTIR spectra were obtained by means of integration

$$I = \int \sigma(\upsilon)\, \mathrm{d}\upsilon \tag{1}$$

where σ is the absorption cross section at wavenumber υ. The results given in this work were obtained by averaging the integration results over a variety of spectra. The relative intensities were calculated accordingly. However, integration could not be performed for some bands where overlap is strong. In these cases, absolute intensities were not determined, while relative intensities were estimated from a comparison of the height of the strongest, fairly sharp peaks (e.g., Q branches) of the overlapped band and a band amenable to integration. It should be pointed out that the uncertainties of the experimental intensities are quite large. The uncertainties of experimental absolute intensities are estimated to be less than 50% for the bands of medium intensity and less than 100% for the others.

Absolute intensities of the $7\upsilon_1$ and $8\upsilon_1$ bands were determined earlier[19] by means of intracavity laser absorption spectrometry (ICLAS) and reported as

$$G = \int \sigma(\upsilon)\, \mathrm{d}(\ln \upsilon) \tag{2}$$

The relationship between these two definitions is approximately as follows:

$$I = G\upsilon_0 \tag{3}$$

where υ_0 denotes the band center of the transition. To make comparisons, we computed the intensities *I* for the ICLAS spectra from eq 3. The uncertainties of intensities of the $7\upsilon_1$ and $8\upsilon_1$ bands were reported to be 30%.

Dipole Moment Surface

The ab initio calculations were carried out at the CCSD(T) level (coupled cluster theory with all single and double substitutions from the Hartree−Fock reference determinant[28] augmented by a perturbative treatment of connected triple excitations[29,30]) using the correlation-consistent polarized valence quadruple-ζ cc-pVQZ basis set.[31] The calculations employed the Molpro2000 package[32,33] both for geometry optimization and for single-point calculations to generate the DMS.

The optimized equilibrium Si−H bond length is $R_{SiH} = 1.47983$ Å. The dipole moment was calculated numerically as energy derivative by finite difference. A finite dipole field was added to the one-electron Hamiltonian. The field strength was chosen to be 0.005 au. Actually, a variety of values for the field strength were tested (ranging between 0.002 and 0.01 au), but the differences between the resulting molecular dipole moments were negligible. When generating the DMS, we kept the SiD_3 frame fixed at its equilibrium configuration. For the one-dimensional DMS, the dipole moments were calculated as a function of the Si−H bond length displacement. In the case of the three-dimensional DMS, the Si−H stretching and two orthogonal Si−H bending motions were taken into consideration.

It should be stressed that our internal coordinate model neglects the contributions of motions of the SiD_3 frame to the DMS and the force field (section IV). The normal-coordinate models (without frozen SiD_3 frame) allow for such contributions and therefore tend to be superior for low dimensional subspaces.[9,34,35] Such models have been applied successfully in elaborate spectroscopic and quantum dynamical studies of the Fermi resonance in CHD_3.[36−38] On the other hand, the internal coordinate model has been shown to reproduce the vibrational energy levels and infrared intensities of CHD_3 quite well,[10] implying that it may be a good first approximation to neglect the effect of harmonic coupling between the C−H chromophore and the CD_3 frame vibrations in CHD_3.[10] We expect that this also applies to $SiHD_3$.

For the one-dimensional DMS calculation, 30 data points were obtained by scanning the Si−H bond length displacement $r = R - R_e$ in steps of 0.05 Å ranging from −0.6 to 0.85 Å, where *R* denotes the instantaneous Si−H bond length and R_e the equilibrium bond length. The corresponding CCSD(T) dipole moments are generally close to those computed previously by a density functional method.[39] The differences between these two data sets are small when the displacement is small but become larger as the displacement increases. We expect that the high-level CCSD(T) method used here yields more accurate results, though it might also start to diverge if the bond is sufficiently stretched.

We find that the DMS of $SiHD_3$ does not possess a strong nonlinearity as in the case of $CHCl_3$,[40] $CHBr_3$,[41] and CHI_3.[42] As the asymptotic behavior for $R \rightarrow \infty$ is unimportant for our intensity calculation,[40,43,44] a polynomial function up to the fifth order was employed to fit the DMS

$$M_z(r) = \sum_{m=1}^{5} C^z_{m00} r^m \tag{4}$$

Here, M_z is the dipole moment component along the molecular C_{3v} axis, and C^z_{m00} is an expansion coefficient. Despite the poor asymptotic behavior, a good fit has been achieved for these

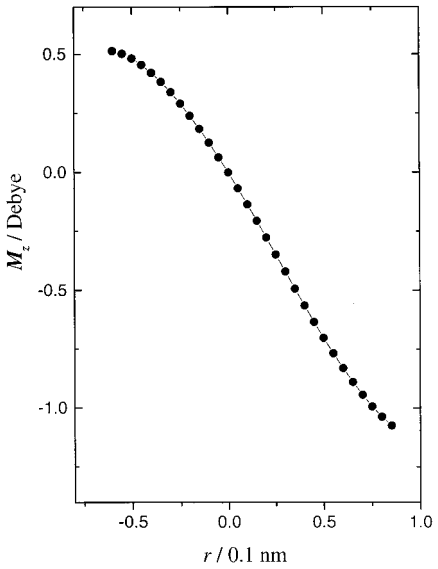

Figure 1. One-dimensional dipole moment surface (M_z) of $SiHD_3$.

data points (see Figure 1). The fitted parameters denoted as 1D-DMS are listed in Table 1.

When calculating the three-dimensional DMS, we generated the grids by scanning the bond length displacement r in steps of 0.10 Å ranging from −0.40 to 0.40 Å (z direction) and two orthogonal (x,y) H−Si-D angle displacements $\Delta\phi_i = \phi_i - \phi_{ie}$ in steps of 2° ranging from −8° to 8°, where ϕ_i and ϕ_{ie} ($i = 1$ and 2) denote the instantaneous and equilibrium i-th H−Si−D angles. The third H−Si−D angle ϕ_3 depends on ϕ_1 and ϕ_2. We point out that our scanning steps are larger than those typically applied in force field calculations due to the fact that we must find a compromise between a wide scanning range and a small number of data points. We checked that the scanning steps used presently are sufficient to produce realistic results. In total, 405 data points were calculated. The raw data were transformed into symmetrized internal coordinates

$$\theta_1 = (2\Delta\phi_1 - \Delta\phi_2 - \Delta\phi_3)/\sqrt{6}$$
$$\theta_2 = (\Delta\phi_2 - \Delta\phi_3)/\sqrt{2} \quad (5)$$

The dipole moment vector **M** has three components, M_x, M_y, and M_z, x, y, and z being the principal inertial axes in the equilibrium configuration. We found that the axes of the Eckart frames are almost superimposed to the principal inertial axes due to the small bending angles. This suggests that the principal inertial axes reference system used in this work are a good approximation to the Eckart reference frame.[45−49]

According to the dipole transition selection rules for molecules of C_{3v} point group, the M_z component leads to totally symmetric (A_1) transitions, while the M_x and M_y components give rise to E symmetry transitions. All components are expanded in symmetrized internal coordinates. This treatment is different from the expansion of DMS in rectilinear normal coordinates. The expansion formulas are as follows:[50]

$$M_z(r,\theta_1,\theta_2) = \sum_m \sum_{p-q=3n} C^z_{mpq} r^m \left(\frac{\theta_+^p\,\theta_-^q + \theta_+^q\,\theta_-^p}{2}\right) \quad (6)$$

$$M_x(r,\theta_1,\theta_2) = \sum_m \sum_{p-q=3n\pm1} C^x_{mpq} r^m \left(\frac{\theta_+^p\,\theta_-^q + \theta_+^q\,\theta_-^p}{2}\right) \quad (7)$$

$$M_y(r,\theta_1,\theta_2) = \sum_m \sum_{p-q=3n\pm1} C^y_{mpq} r^m \left(\frac{\theta_+^p\,\theta_-^q + \theta_+^q\,\theta_-^p}{2i}\right) \quad (8)$$

where C^x_{mpq}, C^y_{mpq}, and C^z_{mpq} are expansion coefficients, m, p, and q are zero or positive integers, $p - q \geq 0$, and $\theta\pm = \theta_1 \pm i\theta_2$. The relationship between the expansion coefficients of the M_x and M_y components is as follows:

$$C^x_{mpq} = C^y_{mpq}, \text{ when } p - q = 3n + 1 \quad (9)$$

$$C^x_{mpq} = -C^y_{mpq}, \text{ when } p - q = 3n - 1 \quad (10)$$

where n is zero or a positive integer. Such a relationship is helpful in fitting the M_x and M_y components.

In practice, it is unnecessary to include many high-order terms in the fit of the three-dimensional DMS, since the accuracy of the ab initio DMS may not be sufficient to determine high-order terms. The results for M_x and M_y components are listed in Table 1 in the second column. For the M_z component, two sets of expansion coefficients were obtained, with the C^z_{030} term being included in the first set (denoted as 3D-DMS_1) and omitted in the second (denoted as 3D-DMS_2). Inclusion of more terms does not reduce the RMS values significantly and has negligible effect on the intensity calculations.

Internal Coordinate Force Field

A reduced three-dimensional Hamiltonian model in terms of curvilinear internal coordinates[11] has been applied in the present study. Only the SiH stretching and bending vibrations are included. Here, we give just a brief description of the model and refer to the literature for details.[11] The vibrational Hamiltonian takes the form

$$H = T + V \quad (11)$$

where

$$T = \frac{1}{2}g_{rr}p_r^2 + \frac{1}{2}g^0_{\theta\theta}\,p_\theta^2 + \frac{1}{2\sqrt{6}}g_6(p_+\theta_+p_+ + p_-\theta_-p_-) + \frac{1}{24}(g_4 + 2g_5)(p+\theta_-^2p_+ + p_-\theta_+^2p_-) + \frac{1}{24}(2g_4 + g_5 + 3g_7)(p_+\theta_-\theta_+p_- + p_-\theta_-\theta_+p_+) + \frac{1}{2}a^{-1}\,g_1yp_\theta^2 + \frac{1}{2}g_2p_r[(\theta_1p_{\theta_1} + \theta_2p_{\theta_2}) + (p_{\theta_1}\theta_1 + p_{\theta_2}\theta_2)] + \frac{1}{4}(a^{-2}g_3 + a^{-1}g_1)y^2p_\theta^2 \quad (12)$$

and

$$V = D_e y^2 + \frac{1}{2}F_{\theta\theta}\theta^2 + \frac{1}{12}F_{\theta\theta\theta}(\theta_+^3 + \theta_-^3) + \frac{1}{24}F_{\theta\theta\theta\theta}\theta^4 + \frac{1}{2}a^{-1}F_{r\theta\theta}y\theta^2 + \frac{1}{4}(a^{-2}F_{rr\theta\theta} + a^{-1}F_{r\theta\theta})y^2\theta^2 \quad (13)$$

In the above equations, the curvilinear internal Si−H stretching displacement coordinate is denoted r, and θ_1 and θ_2 are the symmetrized Si−H bending coordinates, as mentioned above. Here, p_r is the momentum conjugate to r, and p_{θ_1} and p_{θ_2} are the momenta conjugates to θ_1 and θ_2, respectively; $p_\theta^2 = p_{\theta_1}^2 + p_{\theta_2}^2$, $p_\theta\pm = p_{\theta_1} \pm ip_{\theta_2}$, and $\theta^2 = \theta_1^2 + \theta_2^2$. The Morse coordinate is denoted as $y = 1 - \exp(-ar)$, where a is the Morse parameter. Explicit expressions for the kinetic energy expansion coefficients g_{rr}, $g^0_{\theta\theta}$, and g_i(i = 1, 2, ..., 7) are given in detail elsewhere.[11]

TABLE 1: Expansion Coefficients of the One- and Three-dimensional Dipole Moment surfaces for $SiHD_3$ Obtained by Fitting to the ab initio Data Points[a]

	M_x and M_y		M_z		
coefficients	3D-DMS	coefficients	1D-DMS	3D-DMS$_1$	3D-DMS$_2$
$C^x_{010} = C^y_{010}$ (D rad^{-1})	1.25327(52)	C^z_{000} (D)	0.0	0.0	0.0
$C^x_{020} = -C^y_{020}$ (D rad^{-2})	0.00436(60)	C^z_{011} (D rad^{-2})	−	0.4589 (16)	0.4510 (23)
$C^x_{021} = C^y_{021}$ (D rad^{-3})	−0.2817 (27)	C^z_{030} (D rad^{-3})	−	−0.0402 (18)	−
$C^x_{031} = -C^y_{031}$ (D rad^{-4})	0.083 (27)	C^z_{022} (D rad^{-4})	−	−0.023 (16)	0.096 (22)
$C^x_{040} = C^y_{040}$ (D rad^{-4})	0.0231 (27)	C^z_{100} (DÅ^{-1})	−1.3130 (11)	−1.31048 (23)	−1.31048 (34)
$C^x_{110} = C^y_{110}$ (DÅ^{-1} rad^{-1})	0.16305(24)	C^z_{111} (DÅ^{-1} rad^{-2})	−	0.1514 (26)	0.1514 (40)
$C^x_{120} = -C^y_{120}$ (DÅ^{-1} rad^{-2})	−0.0566 (24)	C^z_{200} (DÅ^{-2})	−0.4427 (38)	−0.4618 (11)	−0.4600 (17)
$C^x_{121} = C^y_{121}$ (DÅ^{-1} rad^{-3})	−0.0187 (10)	C^z_{211} (DÅ^{-2} rad^{-2})	−	0.226 (10)	0.215 (16)
$C^x_{210} = C^y_{210}$ (DÅ^{-2} rad^{-1})	0.2683 (28)	C^z_{300} (DÅ^{-3})	0.4882 (74)	0.4814 (16)	0.4814 (24)
$C^x_{220} = C^y_{220}$ (DÅ^{-2} rad^{-2})	−0.0211 (68)	C^z_{400} (DÅ^{-4})	0.017 (10)	0.1069 (73)	0.100 (11)
$C^x_{310} = C^y_{310}$ (DÅ^{-3} rad^{-1})	−0.0663 (13)	C^z_{500} (DÅ^{-5})	0.121 (14)	−	−
RMS of the residuals (D)	1.2×10^{-4}		6.9×10^{-4}	4.1×10^{-3}	6.1×10^{-3}

[a] The uncertainties given in parentheses are 1 standard error in the last significant digits. See text for details. 1 Å = 10^{-10} m, 1 D = 3.33564×10^{-30} C m.

Definitions of the potential energy parameters D_e, $F_{\theta\theta}$, $F_{\theta\theta\theta}$, $F_{\theta\theta\theta\theta}$, $F_{r\theta\theta}$, and $F_{rr\theta\theta}$ are as customary and have also been given explicitly in the literature. They will not be repeated here.

A FORTRAN code has been developed for the present study, which was utilized to first optimize the potential surfaces by fitting to the observed energy levels and then to calculate the intensities by using the optimized potential surfaces and ab initio DMS. The optimizations were performed by a nonlinear least-squares algorithm.[51] The vibrational wave functions and eigenvalues were calculated variationally. The Morse functions were chosen to be consistent with the parameters a, D_e, and g_{rr}. The harmonic oscillator basis functions were chosen to be consistent with the kinetic coefficient $g_{\theta\theta}$ and force constant $F_{\theta\theta}$. The matrix elements for all terms of the Hamiltonian are given in ref 11. We adopted the described two-step procedure[11] to reduce the sizes of the Hamiltonian matrices. The basis sets[11] were constructed as follows: The maximum vibrational quantum number for the stretching and bending modes were $n_1 = 10$ and $n_5 = 30$, respectively. The maximum vibrational angular momentum quantum number for the bending mode was $l = 6$. The highest zero-order energy of the pure bending basis functions was 27 000 cm^{-1}, while that of the stretching—bending basis functions was 36 000 cm^{-1}.

In total 15 experimental band centers[12] were used as input data, with the one at 2531 cm^{-1} being omitted due to large experimental uncertainty (see also Table 4 below). Standard weights of 1.0 were assigned to all data, expect for two overlapped bands at 1690 and 5943 cm^{-1} that were given smaller weights (0.2). The cubic bending term $F_{\theta\theta\theta}$ which will couple states with different vibrational angular momentum numbers was constrained to zero because there is at present no experimental evidence for this kind of coupling. To overcome the strong correlation between $F_{r\theta\theta}$ and $F_{rr\theta\theta}$, we adopted the method[11] to constrain $F_{rr\theta\theta}$ and the whole coefficient of the $y^2\theta^2$ term to zero. This treatment removed the interdependence and yielded a fit with a root-mean-square (RMS) deviation value of 0.66 cm^{-1}, which is smaller than the experimental uncertainty. The kinetic coefficients and optimized potential parameters are listed in Table 2. The energy levels of the stretching overtones were also modeled by a Morse oscillator whose parameters were obtained from a fit to the experimental data.[12] The results are $\omega = 2253.92(18)$ cm^{-1}, and $\omega x = 33.559(21)$ cm^{-1}, with an RMS = 0.365 cm^{-1}. The uncertainties given in parentheses are 1 standard error in the last significant digits.

Consistent with the results of the recent CVPT study,[26] the Fermi coupling between the Si−H stretching and bending motions is unimportant for $SiHD_3$, and the corresponding wave functions mix only very slightly. The reason for this very small stretching-bending coupling is the cancellation of contributions from the kinetic and the potential coupling terms. This can be understood as follows. By checking the Hamiltonian matrix elements, we find that the kinetic coupling term, $(^1/_2)a^{-1}g_1yp_\theta^2$, and the potential coupling term, $(^1/_2)a^{-1}F_{r\theta\theta}y\theta^2$, dominate the Fermi interactions. The corresponding matrix elements are (vibrational angular momentum $l = 0$ assumed for simplification)

$$\langle v_b|p_\theta^2|v_{b+2}\rangle = -[(v_b + 2)/2]\alpha_\theta$$
$$\langle v_b|\theta^2|v_{b+2}\rangle = +[(v_b + 2)/2]\alpha_\theta^{-1} \qquad (14)$$

where $\alpha_\theta = (F_{\theta\theta}/g^0_{\theta\theta})^{1/2}/\hbar$, so the sum of the kinetic and potential interaction terms is $(^1/_4)a^{-1}y(v_b + 2)[-g_1\alpha_\theta + F_{r\theta\theta}\alpha_\theta^{-1}]$ in this case. The expression in square brackets is evaluated in Table 3 for $SiHD_3$ and also for $SiHF_3$.[52] There are two obvious points: First, the matrix element contributions from the kinetic and potential terms are of opposite sign. Second, the absolute values of these contributions are comparable, resulting in significant cancellation, which is even more pronounced for $SiHD_3$ than for $SiHF_3$. Thus, the Fermi resonances involving Si−H stretching and bending motions are unimportant for $SiHD_3$ and $SiHF_3$. This implies a slow energy redistribution between the stretching and bending motions[3] and contributes to the local mode character of these vibrations.

It is interesting to note that early work on resonances in CO_2,[53] CHF_3, and $CHCl_3$[54] suggested a dominance of kinetic energy

TABLE 2: Kinetic Coefficients and Optimized Potential Energy Parameters for $SiHD_3$[a]

kinetic		potential	
g_{rr} (u^{-1})	1.027 98	D_e (aJ)	0.76104 (44)
$g^0_{\theta\theta}$ (u^{-1} Å^{-2})	0.951338	a (Å^{-1})	1.39200 (54)
g_1 (u^{-1} Å^{-3})	−0.964861	ω (cm^{-1})	2268.415
g_2 (u^{-1} Å^{-1})	0.00805744	ωx (cm^{-1})	33.578
g_3 (u^{-1} Å^{-4})	1.950 03	$F_{\theta\theta}$ (aJ)	0.4631 (17)
g_4 (u^{-1} Å^{-2})	0.389380	$F_{\theta\theta\theta}$ (aJ)	0[b]
g_5 (u^{-1} Å^{-2})	−0.660982	$F_{\theta\theta\theta\theta}$ (aJ)	0.618 (94)
g_6 (u^{-1} Å^{-2})	0.286892	$F_{r\theta\theta}$(aJ Å^{-1})	−0.372 (11)
g_7 (u^{-1} Å^{-2})	−0.383931	$F_{rr\theta\theta}$ (aJ Å^{-2})	0[b]

[a] Definitions of the kinetic parameters are given in ref 11. The uncertainties given in parentheses are standard error in the last significant digit. The atomic mass unit is au, 1 Å = 10^{-10} m, and 1 aJ = 10^{-18} J. [b] Constrained to zero; see text for details.

TABLE 3: Some Selected Approximate Values of Kinetic Coefficients and Potential Parameters for $SiHD_3$ and $SiHF_3$ Species[a]

	g_1 (u^{-1} Å^{-3})	$F_{r\theta\theta}$ (aJ Å^{-1})	$g^0_{\theta\theta}$ (u^{-1} Å^{-2})	$F_{\theta\theta}$ (aJ)	α_θ (aJ$^{1/2}$ u$^{1/2}$ Å)	$F_{r\theta\theta}\alpha_\theta^{-1} - g\alpha_{1\theta}$ (aJ$^{1/2}$ u$^{-1/2}$ Å^{-2})
$SiHD_3$	−0.9649	−0.3720	0.9513	0.4631	0.6977	−0.5331 + 0.6732 = 0.1401
$SiHF_3$	−1.0258	−0.4740	0.7757	0.5548	0.8457	−0.5605 + 0.8675 = 0.3070

[a] Data for $SiHF_3$ from ref 52. The atomic mass unit is au, 1 Å = 10^{-10} m, 1 aJ = 10^{-18} J, and $\alpha_\theta = (F_{\theta\theta}/g^0_{\theta\theta})^{1/2}/\hbar$.

coupling over potential energy coupling in curvilinear coordinate models. A later theoretical survey study[55] for a larger set of molecules showed, however, that the potential coupling terms are not negligible in general and that their contributions are needed for quantitative predictions and sometimes even for qualitative purposes. The experimental finding for $SiHD_3$ and $SiHF_3$ in the present contribution supports the conclusion that Fermi resonances cannot be described by kinetic coupling alone.

Intensity Calculations

The absolute vibrational band intensity I can be calculated as

$$I = \frac{8\pi^3 \nu_0}{3hcQ_v(T)}\left[1 - \exp\left(-\frac{hc\nu_0}{kT}\right)\right]|\langle N|\mathbf{M}|0\rangle|^2 \qquad (15)$$

Here $|0\rangle$ and $|N\rangle$ denote the vibrational ground and excited states, respectively, ν_0 is the transition wavenumber in cm^{-1}, T is the sample temperature in the measurement, $Q_v(T)$ is the vibrational partition function at temperature T, c is the speed of light, and k and h are Boltzmann and Planck constants, respectively. Approximately, $[1 - \exp(-hc\nu_0/kT)] \simeq 1$ and $Q_v(T) \simeq 1$ hold. The parallel band intensity $I_{||}$ and perpendicular band intensity $I_\perp$ are thus given as

$$I_{||} = \frac{8\pi^3\nu_0}{3hc}|\langle N|M_z|0\rangle|^2 = K\nu_0\left|\frac{\langle N|M_z|0\rangle}{\text{Debye}}\right|^2$$

$$I_\perp = \frac{8\pi^3\nu_0}{3hc}\left|\frac{\langle N|M_x|0\rangle}{\text{Debye}}\right|^2 + \frac{8\pi^3\nu_0}{3hc}\left|\frac{\langle N|M_y|0\rangle}{\text{Debye}}\right|^2$$

$$= K\nu_0\left(\left|\frac{\langle N|M_x|0\rangle}{\text{Debye}}\right|^2 + \left|\frac{\langle N|M_y|0\rangle}{\text{Debye}}\right|^2\right) \qquad (16)$$

Here, $K = 4.162\,375\,5 \times 10^{-19}$ cm^2 (making use of 1 D ≡ 1 D = 10^{-18} $(dyn)^{1/2}$ cm^2 in the cgs system, corresponding to $3.335\,64 \times 10^{-30}$ C m in SI units.[34]) The result can be further converted into the unit of cm^{-2} ATM^{-1} by multiplying with a factor of 2.6867×10^{19}.

In a similar way, which is detailed in ref 40, the intensities can be obtained with different models:

(i) "Single Morse" (SM) model. A simple Morse function is used to describe the Si−H stretching vibration motion, without considering the bending modes. Both the ground and excited states are assumed to be pure stretching states, and only the one-dimensional DMS is used in this model. The Morse parameters have been given in section IV.

(ii) "1D" model. A Morse function is used to describe the Si−H stretching vibration motion, and harmonic oscillator basis functions are used for the bending modes. The reduced three-dimensional Hamiltonian model described above is applied. The ground state is $|v_s = 0, v_b = 0>$ and the excited state is $|v_s = n_1, v_b = n_5>$. The one-dimensional DMS is used in this model.

(iii) "3D" model. This is analogous to the "1D" model, but the three-dimensional DMS is used.

The intensities both of parallel and perpendicular bands were calculated. The needed matrix elements are given explicitly in refs 8, 42, and 50. The relative intensities were determined as I/I_{ν_1}. For the parallel bands, 1D-DMS was employed in the SM and 1D models, with the results being denoted SM and 1D, respectively, while both 3D-DMS_1 and 3D-DMS_2 were used in the 3D model, with the respective results being referred to as $3D_1$ and $3D_2$. Since the $3D_1$ and $3D_2$ results are almost identical, we only present the former under the label 3D. For the perpendicular bands, there is only one set of 3D-DMS, and the results are again labeled as 3D. The absolute intensities are given in Table 4, and intensities relative to ν_1 are listed in Table 5. The experimental intensities are also given.

There are several points concerning the results which should be noted.

First, the overall agreement between the calculations and observations is reasonable both for absolute and relative intensities, although the calculation is still not of experimental accuracy. The agreement is most satisfactory for all perpendicular bands, and also for parallel bands with low excitations. This can be seen from Tables 4 and 5 and also from Figure 2, where relative intensities are displayed. The intensities of the stretching bands $I_{n\nu_1}$ calculated by the SM, 1D, and 3D models are close to each other. Therefore, when only such bands are considered, all three models are applicable. The SM model is particularly simple and easy to implement and, thus, can be used as a good first-order approximation for semiquantitative predictions.

Second, it is interesting to see that the intensities of the stretching bands decrease rapidly from the ν_1 to the $3\nu_1$ bands by a factor greater than 100 in each step. However, the intensity of the $4\nu_1$ band is on the same order as and even slightly larger than that of $3\nu_1$. The experimental ratio $I_{3\nu_1}/I_{4\nu_1}$ is about 0.56. The predicted values are 1.07, 0.92, and 0.80 for the SM, 1D, and 3D models, respectively. This behavior is caused by the cancellation of the contributions from the linear C^z_{100} and quadratic C^z_{200} terms in the DMS, which has been discussed in more detail elsewhere.[52] Here we give only a brief explanation: Compared with the C^z_{100} term, the relative contributions from higher-order terms such as C^z_{200} increase rapidly as excitation increases and cannot be neglected except for the case $n_1 = 1$. These two contributions have opposite signs when $n_1 > 1$, which results in a strong cancellation and a rapid decrease of intensity for $2\nu_1$ and $3\nu_1$ transition. When $n_1 \geq 3$, the cancellation is so significant that the third-order term C^z_{300} becomes important or even dominant. The overall cancellation effect is more serious for $n_1 = 3$ than for $n_1 = 4$, such that $3\nu_1$ becomes weaker than $4\nu_1$.

Finally, it can be seen that the stretching $n_1\nu_1$ bands are usually much stronger than the stretching-bending $(n_1 - 1)\nu_1 + 2\nu_5$ combination bands. However, the intensity of the $3\nu_1$ band is found to be comparable with that of the $2\nu_1 + 2\nu_5$ band, as is evident from Figure 3, where the intensities of the $n_1\nu_1$ and $(n_1 - 1)\nu_1 + 2\nu_5$ bands are compared. The experimental ratio $I_{2\nu_1+2\nu_5}$:$I_{3\nu_1}$ is about 0.43:0.57. The 1D model cannot reproduce this observation because the bending motion has been neglected in the one-dimensional DMS. As a result, the Si−H stretching will carry all strength of the transition, and the stretching-bending combinations can only borrow some intensity

TABLE 4: Observed and Calculated Absolute Band Intensities of $SiHD_3$[a]

				I (cm^{-2} ATM^{-1})			
sym.	$\tilde{\nu}_{obs}$ (cm^{-1})	assignment	$\tilde{\nu}_{cal}$ (cm^{-1})	obs	SM	1D	3D[b]
A_1	1690[c]	$2\nu_5$	1693.294		−	0.12	7.0
	2187.207	ν_1	2186.807	255	335	336	331
	−	$4\nu_5$	3363.202	−	−	0.31×10^{-3}	0.17×10^{-2}
	3852	$\nu_1 + 2\nu_5$	3851.273	−	−	0.84×10^{-3}	0.20×10^{-1}
	4307.09	$2\nu_1$	4306.462	1.02	1.76	1.83	1.69
	5943[c]	$2\nu_1 + 2\nu_5$	5942.115	−	−	0.21×10^{-4}	0.12×10^{-2}
	6359	$3\nu_1$	6358.966	0.84×10^{-3}	0.47×10^{-2}	0.39×10^{-2}	0.42×10^{-2}
	−	$3\nu_1 + 2\nu_5$	7965.828	−	−	0.11×10^{-4}	0.76×10^{-4}
	8344	$4\nu_1$	8344.322	0.15×10^{-2}	0.46×10^{-2}	0.44×10^{-2}	0.49×10^{-2}
	−	$5\nu_1$	10262.535	−	0.91×10^{-3}	0.88×10^{-3}	0.89×10^{-3}
	12111.39	$6\nu_1$	12113.614	−	0.15×10^{-3}	0.15×10^{-3}	0.13×10^{-3}
	13897.51	$7\nu_1$	13897.580	0.34×10^{-4}	0.25×10^{-4}	0.24×10^{-4}	0.20×10^{-4}
	15614.66	$8\nu_1$	15614.555	0.13×10^{-5}	0.45×10^{-5}	0.43×10^{-5}	0.31×10^{-5}
	17265.70	$9\nu_1$	17265.601	−	0.85×10^{-6}	0.83×10^{-6}	0.53×10^{-6}
E	850.681	ν_5	851.268	357	−	−	536
	2531[d]	$3\nu_5$	2533.202	−	−	−	0.27
	3024	$\nu_1 + \nu_5$	3023.654	1.77	−	−	0.74
	−	$\nu_1 + 3\nu_5$	4676.770	−	−	−	0.19×10^{-2}
	5130	$2\nu_1 + \nu_5$	5128.893	0.80×10^{-1}	−	−	0.71×10^{-1}
	−	$2\nu_1 + 3\nu_5$	6753.215	−	−	−	0.48×10^{-4}
	7165	$3\nu_1 + \nu_5$	7166.991	0.60×10^{-2}	−	−	0.60×10^{-2}
	−	$4\nu_1 + \nu_5$	9137.954		−	−	0.54×10^{-3}

[a] Experimental data are the same as those in refs 12 and 19. See these references for more details. No experimental data are given for those bands which are either not covered by the spectral window or buried in other strong absorptions (e.g., water absorptions). The results obtained by use of the SM, 1D, and 3D models are denoted as SM, 1D, and 3D, respectively. [b] $3D_1$ results for the parallel bands (see text). The $3D_2$ results differ negligibly in 12 out of 14 cases, slightly for $3\nu_1 + 2\nu_5$ ($0.70E-4$) and significantly only for $4\nu_5$ (0.31×10^{-3}), indicating that the C^z_{030} term is not overly important (see section III). [c] Given a weight of 0.2 in the force field fitting. [d] Not used in the force field fitting due to large uncertainty.

TABLE 5: Observed and Calculated Relative Band Intensities of $SiHD_3$[a]

				I/I_{ν_1}			
sym.	$\tilde{\nu}_{obs}$ (cm^{-1})	assignment	$\tilde{\nu}_{cal}$ (cm^{-1})	obs	SM	1D	3D[b]
A_1	1690[c]	$2\nu_5$	1693.294	0.14×10^{-1} [d]	−	0.35×10^{-3}	0.21×10^{-1}
	2187.207	ν_1	2186.807	1.00	1.00	1.00	1.00
	−	$4\nu_5$	3363.202	−	−	0.10×10^{-5}	0.46×10^{-5}
	3852	$\nu_1 + 2\nu_5$	3851.273	0.14×10^{-3} [d]	−	0.25×10^{-5}	0.60×10^{-4}
	4307.09	$2\nu_1$	4306.462	0.40×10^{-2}	0.53×10^{-2}	0.54×10^{-2}	0.51×10^{-2}
	5943[c]	$2\nu_1 + 2\nu_5$	5942.115	0.25×10^{-5} [d]	−	0.59×10^{-7}	0.37×10^{-5}
	6359	$3\nu_1$	6358.966	0.33×10^{-5}	0.15×10^{-4}	0.12×10^{-4}	0.13×10^{-4}
	−	$3\nu_1 + 2\nu_5$	7965.828	−	−	0.32×10^{-7}	0.22×10^{-6}
	8344	$4\nu_1$	8344.322	0.59×10^{-5}	0.14×10^{-4}	0.13×10^{-4}	0.15×10^{-4}
	−	$5\nu_1$	10262.535	−	0.29×10^{-5}	0.26×10^{-5}	0.27×10^{-5}
	12111.39	$6\nu_1$	12113.614	−	0.49×10^{-6}	0.42×10^{-6}	0.40×10^{-6}
	13897.51	$7\nu_1$	13897.580	0.13×10^{-6}	0.83×10^{-7}	0.71×10^{-7}	0.60×10^{-7}
	15614.66	$8\nu_1$	15614.555	0.51×10^{-8}	0.15×10^{-7}	0.13×10^{-7}	0.94×10^{-8}
	17265.70	$9\nu_1$	17265.601	−	0.29×10^{-8}	0.25×10^{-8}	0.16×10^{-8}
E	850.681	ν_5	851.268	1.40	−	−	1.62
	2531[d]	$3\nu_5$	2533.202	0.49×10^{-3} [d]	−	−	0.82×10^{-3}
	3024	$\nu_1 + \nu_5$	3023.654	0.69×10^{-2}	−	−	0.22×10^{-2}
	−	$\nu_1 + 3\nu_5$	4676.770	−	−	−	0.54×10^{-5}
	5130	$2\nu_1 + \nu_5$	5128.893	0.31×10^{-3}	−	−	0.21×10^{-3}
	−	$2\nu_1 + 3\nu_5$	6753.215	−	−	−	0.13×10^{-6}
	7165	$3\nu_1 + \nu_5$	7166.991	0.24×10^{-4}	−	−	0.18×10^{-4}
	−	$4\nu_1 + \nu_5$	9137.954		−	−	0.16×10^{-5}

[a] See text for details. The notation is defined in footnote a of Table 4. [b] $3D_1$ results for the parallel bands (see text). The $3D_2$ results differ negligibly in 12 out of 14 cases, slightly for $3\nu_1 + 2\nu_5$ ($0.20E-6$), and significantly only for $4\nu_5$ ($0.10E-5$). [c] Given a weight of 0.2 in the force field fitting. [d] Estimated values of larger uncertainty. [e] Not used in the force field fitting due to large uncertainty.

from the pure stretching overtones through resonances. That is, the relative band intensities are largely determined by the pure stretching character of the true eigenfunction of each band. As the Fermi resonance is insignificant and the wave function mixture is small, the ratio of $I_{(n_1-1)\nu_1+2\nu_5}$:$I_{n\nu_1}$ is very small. The calculations by the 1D model give $I_{2\nu_1+2\nu_5}$:$I_{3\nu_1} \simeq 0.005$:0.995. However, the 3D calculations yield much better agreement with the experiment, with $I_{2\nu_1+2\nu_5}$:$I_{3\nu_1} \simeq 0.22$:0.78. This confirms the importance of the bending motion in the multidimensional DMS for intensity investigations.[40−42]

Summary

In this work, we report on the internal coordinate force field and overtone band intensities for the Si−H chromophore in the $SiHD_3$ molecule. The potential parameters were optimized by fitting to the experimental band centers. The insignificance of the Fermi resonance between the Si−H stretching and bending motions is found to arise from cancellation of the contributions from kinetic and potential terms, which favors local mode character. The band intensities were calculated by using ab initio

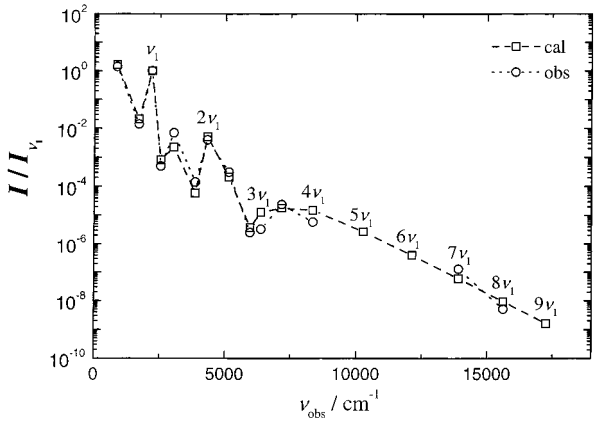

Figure 2. Relative intensities of Si−H stretching-bending polyads of $SiHD_3$. The circles indicate the observed values. The values calculated from the 3D model are denoted by squares. The 3D-DMS_1 was used for the parallel bands.

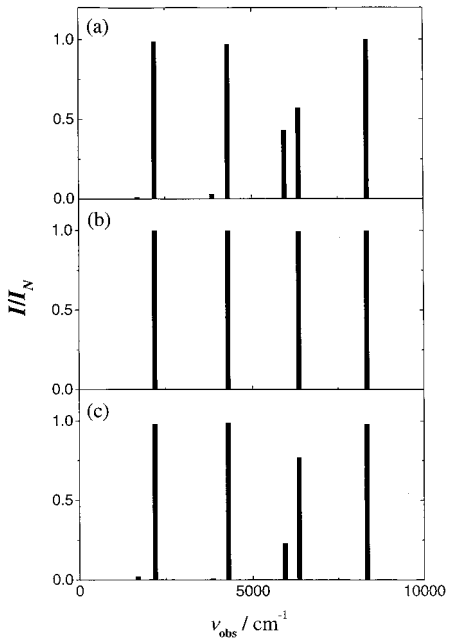

Figure 3. Relative intensities of the $n_1\nu_1$ and $(n_1 - 1)\nu_1 + 2\nu_5$ bands of $SiHD_3$ calculated as $I_{n_1\nu_1}/I_N$ and $I_{(n_1-1)\nu_1+2\nu_5}/I_N$, where $I_N = I_{n_1\nu_1} + I_{(n_1-1)\nu_1+2\nu_5}$. (a) Experimental data. (b) 1D model result. (c) 3D model result. The $3D_1$ results are shown.

one- and three-dimensional DMS, and they agree reasonably well with observations. The successful reproduction of the relative intensities within the stretching-bending combination $(n_1 - 1)\nu_1 + 2\nu_5$ dyads and the stretching $n_1\nu_1$ bands underlines the importance of the bending motion in the multidimensional DMS for intensity investigations.

Acknowledgment. This work was supported by the National Natural Science Foundation of China (Grants 29903010 and 29892161), the Deutsche Forschungsgemeinschaft (Project Bu 152/17), and EC (Research Training Network HPRN-CT-2000-00022). Hai Lin thanks the Alexander von Humboldt Foundation for a Research Fellowship and Xiao-gang Wang for helpful discussions.

Supporting Information Available: The matrix elements for intensity calculations on perpendicular bands are given in Table 1S. Table 2S contains ab initio one-dimensional DMS data points (M_z component) of $SiHD_3$. The M_x and M_z components of the ab initio three-dimensional DMS of $SiHD_3$ are listed in Table 3S. The ab initio calculations were carried out at the CCSD(T)/cc-pVQZ level using the frozen core approximation. The M_y components of the three-dimensional DMS were not calculated but can be derived by symmetry considerations[CITE:He00JPC]. See also eqs 9 and 10. This material is available free of charge via the Internet at http://pubs.acs.org.

References and Notes

(1) Child, M. S.; Halonen, L. *Adv. Chem. Phys.* **1984**, *57*, 1.
(2) Halonen, L. *Adv. Chem. Phys.* **1998**, *104*, 41.
(3) Quack, M. *Annu. Rev. Phys. Chem.* **1990**, *41*, 839.
(4) Davidsson, J.; Gutow, J. H.; Zare, R. N.; Hollenstein, H. A.; Marquardt, R. R.; Quack, M. *J. Phys. Chem.* **1991**, *95*, 1201.
(5) Marquardt, R. R.; Goncalves, N. S.; Sala, O. *J. Chem. Phys.* **1995**, *103*, 8391.
(6) Carrington, T., Jr.; Halonen, L.; Quack, M. *Chem. Phys. Lett.* **1987**, *140*, 512.
(7) Halonen, L.; Carrington, T., Jr.; Quack, M. *J. Chem. Soc., Faraday Trans. 2* **1988**, *84*, 1371.
(8) Kauppi, E.; Halonen, L. *J. Chem. Phys.* **1989**, *90*, 6980.
(9) Hollenstein, H.; Luckhaus, D.; Quack, M. *J. Mol. Struct.* **1993**, *294*, 65.
(10) Kauppi, E. *J. Chem. Phys.* **1994**, *101*, 6470.
(11) Kauppi, E. *J. Mol. Spectrosc.* **1994**, *167*, 314, and references therein.
(12) Lin, H.; Bürger, H.; Wang, X. G. Unpublished results, 2001.
(13) Boyd, D. R. *J. Chem. Phys.* **1954**, *23*, 922.
(14) Meal, J. H.; Wilson, M. K. *J. Chem. Phys.* **1956**, *24*, 385.
(15) Olson, W. B.; Lovejoy, R. W. *J. Mol. Spectrosc.* **1977**, *66*, 314.
(16) Frommer, C.; Lovejoy, R. W.; Sams, R. L.; Olson, W. B. *J. Mol. Spectrosc.* **1981**, *89*, 261.
(17) Bernheim, R. A.; Lampe, F. W.; O'Keefe, J. F.; Qualey, J. R., III *J. Mol. Spectrosc.* **1984**, *104*, 194.
(18) Schaeffer, R. D.; Lovejoy, R. W.; Olson, W. B.; Tarrago, G. *J. Mol. Spectrosc.* **1988**, *128*, 135.
(19) Campargue, A.; Chenevier, M.; Stoeckel, F. *Chem. Phys.* **1989**, *137*, 249.
(20) Campargue, A.; Chenevier, M.; Stoeckel, F. *Chem. Phys.* **1989**, *138*, 405.
(21) Bürger, H.; Ruland, H.; Fusina, L. *Chem. Phys. Lett.* **1997**, *268*, 249.
(22) Bürger, H.; Jerzembeck, W.; Ruland, H.; Halonen, L. *J. Mol. Spectrosc.* **1998**, *189*, 8.
(23) Bürger, H.; Ruland, H.; Halonen, L. *J. Mol. Spectrosc.* **2000**, *202*, 44.
(24) Ohno, K.; Matsuura, H.; Endo, Y.; Hirota, E. *J. Mol. Spectrosc.* **1985**, *111*, 73.
(25) Ohno, K.; Matsuura, H.; Endo, Y.; Hirota, E. *J. Mol. Spectrosc.* **1986**, *118*, 1.
(26) Wang, X. G.; Sibert, E. L. *J. Chem. Phys.* **2000**, *113*, 5384.
(27) Martin, J. M. L.; Baldridge, K. K.; Lee, T. J. *Mol. Phys.* **1999**, *97*, 945.
(28) Purvis, G. D.; Bartlett, R. J. *J. Chem. Phys.* **1982**, *76*, 1910.
(29) Urban, M.; Noga, J.; Cole, S. J.; Bartlett, R. J. *J. Chem. Phys.* **1985**, *83*, 4041.
(30) Raghavachari, K.; Trucks, G. W.; Pople, J. A.; Head-Gordon, M. *Chem. Phys. Lett.* **1989**, *157*, 479.
(31) Dunning, T. H. *J. Chem. Phys.* **1989**, *90*, 1007. Woon, D. E.; Dunning, T. H. *J. Chem. Phys.* **1993**, *98*, 1358.
(32) Molpro2000 is a package of ab initio programs written by Werner, H.-J.; Knowles, P. J., with contributions from Amos, R. D.; Bernhardsson, A.; Berning, A.; Celani, P.; Cooper, D. L.; Deegan, M. J. O.; Dobbyn, A. J.; Eckert, F.; Hampel, C.; Hetzer, G.; Korona, T.; Lindh, R.; Lloyad, A. W.; McNicholas, S. J.; Mandy, F. R.; Meyer, W.; Mura, M. E.; Nicklass, A.; Palmieri, P.; Pitzer, R.; Rauhut, G.; Schütz, M.; Stoll, H.; Stones, A. J.; Tarroni, R.; Thorsteinsson. T.
(33) Hampel, C.; Peterson, K.; Werner, H.-J. *Chem. Phys. Lett.* **1992**, *190*, 1, and references therein. The program to compute the perturbative triples corrections has been developed by Deegan, M. J. O.; Knowles, P. J. *Chem. Phys. Lett.* **1994**, *227*, 321.
(34) Ha, T. K.; Lewerenz, M.; Marquardt, R. R.; Quack, M. *J. Chem. Phys.* **1990**, *93*, 7697.
(35) Hollenstein, H.; Marquardt, R. R.; Quack, M.; Suhm, M. A. *J. Chem. Phys.* **1994**, *101*, 3588.
(36) Lewerenz, M.; Quack, M. *J. Chem. Phys.* **1988**, *88*, 5408.
(37) Marquardt, R.; Quack, M. *J. Chem. Phys.* **1991**, *95*, 4854.
(38) Marquardt, R.; Quack, M.; Thanopulos, I. *J. Phys. Chem. A* **2000**, *104*, 6129.
(39) Lin, H.; Yuan, L. F.; Zhu, Q. S. *Chem. Phys. Lett.* **1999**, *308*, 137.

(40) Lin, H.; Yuan, L. F.; He, S. G.; Wang, X. G.; Zhu, Q. S. *J. Chem. Phys.* **2000**, *112*, 7484.
(41) Lin, H.; Yuan, L. F.; He, S. G.; Wang, X. G. *J. Chem. Phys.* **2001**, *114*, 8905.
(42) Lin, H.; Yuan, L. F.; He, S. G.; Wang, X. G.; *Chem. Phys. Lett.* **2000**, *332*, 569.
(43) Lin, H.; Yuan, L. F.; Wang, D.; Zhu, Q. S. *Chin. Phys. Lett.* **2000**, *17*, 13.
(44) Kjaergaard, H. G.; Henry, B. R. *J. Chem. Phys.* **1992**, *96*, 4841.
(45) Eckart, C. *Phys. Rev.* **1935**, *47*, 552.
(46) Lawton, R. T.; Child, M. S. *Mol. Phys.* **1980**, *40*, 773.
(47) LeSueur, C. R.; Miller, S.; Tennyson, J.; Sutcliffe, B. T. *Mol. Phys.* **1992**, *76*, 1147.
(48) Gabriel, W.; Reinsch, E.-A.; Rosmus, P.; Carter, S.; Handy, N. C. *J. Chem. Phys.* **1993**, *99*, 897.
(49) Kjaergaard, H. G.; Henry, B. R.; Wei, H.; Lefebvre, S.; Carrington, T., Jr.; Mortensen, O. S.; Sage, M. L. *J. Chem. Phys.* **1994**, *100*, 6228.
(50) He, S. G.; Yuan, L. F.; Lin, H.; Zhu, Q. S.; Wang, X. G. *J. Phys. Chem. A*, submitted for publication.
(51) Halonen, L.; Child, M. S. *Comput. Phys. Commun.* **1988**, *51*, 173.
(52) Lin, H.; Bürger, H.; MKadmi, E. B.; He, S. G.; Yuan, L. F.; Breidung, J.; Thiel, W.; Demaison, J.; Huet, T. R. *J. Chem. Phys.*, in press.
(53) Sibert, E. L.; Hynes, J. T.; Reinhardt, W. P. *J. Phys. Chem.* **1983**, *87*, 2032.
(54) Green, W. H., Jr.; Lawrance, W. D.; Moore, C. B. *J. Chem. Phys.* **1987**, *86*, 6000; **1988**, *88*, 3401.
(55) Gelessus, A.; Thiel, W. *Ber. Bunsen-Ges. Phys. Chem.* **1995**, *99*, 514.